Consideration of ferromagnetic anisotropy in electrical machines built of segmented silicon steel sheets

Fabian Müller, Gregor Bavendiek, Nora Leuning, Benedikt Schauerte and Kay Hameyer

Institute of Electrical Machines (IEM), RWTH Aachen University, Germany, fabian.mueller@iem.rwth-aachen.de

Keywords: Finite Element Method, Anisotropy, Segmentation, Synchronous Machine

Abstract

The reduction of silicon steel waste in the production process of electrical machines is crucial for economic and ecological reasons. A good material utilization is achieved by the segmentation of the rotor and stator of an electrical machine.
The magnetic field calculation needs an accurate material model to consider the segmentation and anisotropic magnetic material behaviour. The basis of the model in this study are measurements of magnetic material anisotropy in a rotational single sheet tester. Finally, the model is applied to a finite element simulation of a segmented synchronous machine.

1 Introduction

The flux guiding material in rotating electrical machines is commonly constructed of non-oriented (NO) electrical steel. It varies strongly in terms of its material characteristic. However, the magnetisability is even for NO material depending on the direction of the magnetic flux. This anisotropic phenomenon may be the reasons why simulations and measurements are sometimes not in good accordance. For the most appropriate selection of a material for an application, this direction dependence of the magnetic flux should be considered.
In segmented machines, the magnetic anisotropy can be exploited to guide the flux along the easy magnetization axis. The commonly used ideal isotropic material modulation is not sufficient. The measurement-based material representation (MBMR), stated in the following, is not based on an algebraic representation and therefore is capable of being directly used in the simulation of electrical machines. Deriving the reluctivity tensor by a multi-dimensional interpolation of the magnetization characteristic takes the angular dependency of the anisotropy into account. The presented MBMR in combination with the Finite Element Method (FEM) is applied to a permanent magnet synchronous machine.

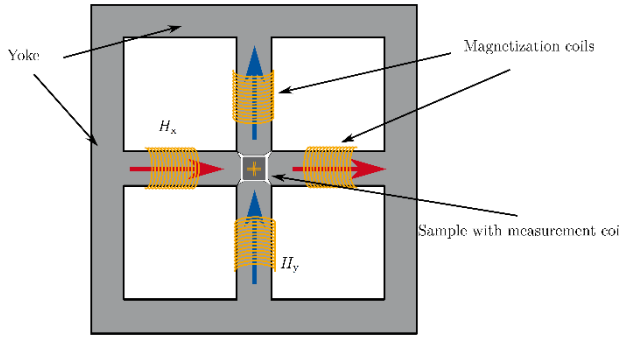

Figure 1: Topology of the utilized Rotational Single Sheet measurement system.

2 Anisotropy

2.1 Basic Theory

Grain oriented (GO) electrical steel shows a very dominant magnetic anisotropy, resulting in a hard and an easy magnetisation axis. Despite this fact the hard axis is for a small magnetic field strength located at the transvers direction and moves with increasing field strength towards the 45-degree direction due to crystal anisotropy [1]. The anisotropy of NO lamination origins mainly from the manufacturing process of the lamination. In the manufacturing process, the strip is rolled and annealed, which affects the location of the magnetic axis and the grain size. Additionally, the anisotropy, due to the crystallographic texture, strongly influences the magnetic characteristics of the final product. The entire magnetisation process can be explained by the domain theory and is depicted in Fig. (2) [2]. In the demagnetized state, most domains are aligned randomly (Point A). Starting from a low applied field those domains, which are oriented along the direction of the applied field grow first by domain wall movement (Point B and C). Further increasing the applied field, domain regions, which are not aligned to the favourable direction, are occupied by properly oriented domains through wall jumps (Point D). Afterwards, the magnetic polarisation can only increase through rotation of the magnetic momentum (Point E). Due to the crystal anisotropy, this rotation needs more magnetic field strength in the 45-degree direction than in the rolling or transverse direction. Taking the anisotropy into account results in a phase shift between the magnetic field strength **H** and the magnetic flux density **B**.

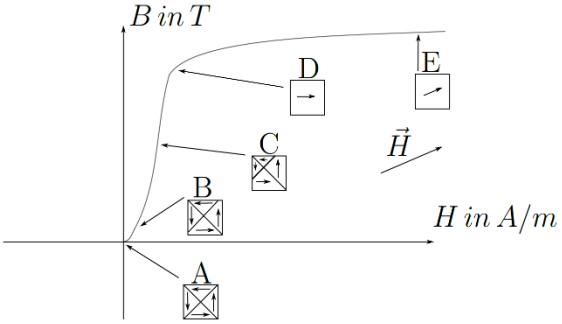

Figure 2: Magnetisation process of a ferromagnetic material.

2.2 Measurements

Measurement to obtain the directional dependent behaviour can be performed in different ways, such as applying unidirectional fields in different direction in a rotational single sheet tester (RSST), or rotating fields in a RSST [4]. The RSST consists of a magnetic yoke and four excitation coils, each fixed on an arm of the yoke, generating the magnetic field. The geometry is depicted in Fig. (1). In this study, the measurements are performed by applying nominal flux densities from 0.1 T to 1.8 T in uniaxial direction and for different excitation angles. This offers the opportunity to measure vectorial characteristics of **B** and **H** with uniaxial measurements [5].

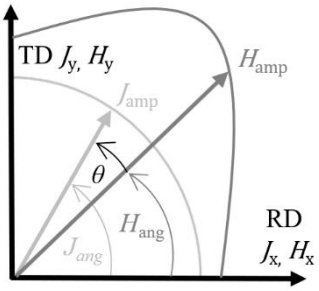

Figure 3: Schematic illustration of the phase shift and vectorial *B* and *H* characteristics.

In order to properly analyze the orientation dependency of the material the angle Θ has to be identified in the measurements. The dependency of the anisotropy to the flux density can be directly depicted from the measurements in Fig. (4). For low flux density amplitudes the anisotropy is comparable to an ellipse, but for high flux densities a deviation from the ellipsoidal shape occurs. For this reason, a simple algebraic approximation of the anisotropy such as an ellipse is not reasonable, even for non-oriented steel sheets. In saturation collinearity can be assumed.
The following measurements in Fig. (4) were conducted for the material Fe-Si 2.4%. The shown measurements can be used to derive an algebraic model from the visible obviously occurring trends. Therefore, the dependency of angle and amplitude needs to be fitted separately and being united into a single anisotropic surface representation.

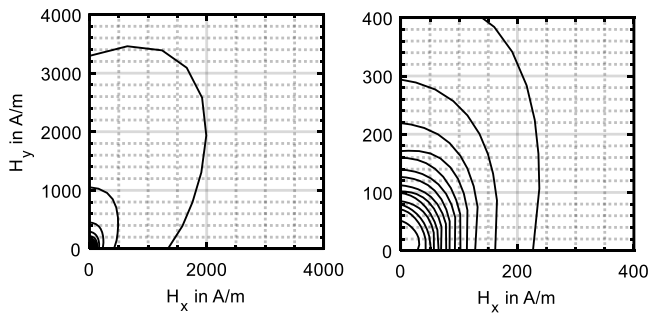

a) H-Loci for different excitations

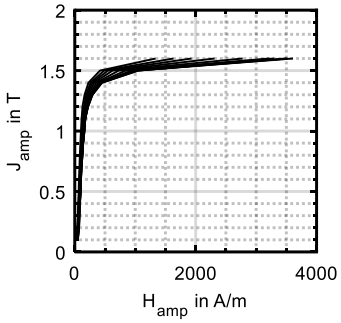

b) $\mathbf{J}_{amp}(\mathbf{H}_{amp})$

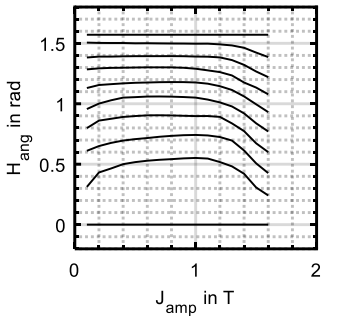

c) $\mathbf{H}_{ang}(\mathbf{J}_{amp})$

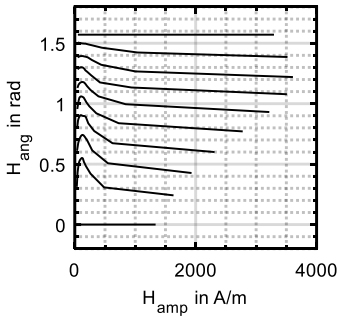

d) $\mathbf{H}_{ang}(\mathbf{H}_{amp})$

Figure 4: Measured magnetic field strength excited by controlled alternating flux densities with a frequency of 50 Hz for Fe-Si 2.4%.

2.3 Measurement Based Material Representation (MBMR)

After the measurement data has been obtained the MBMR is based on expressing the magnetic field strength **H**(B) by a linear combination of surfaces for H_x and H_y $\mathbf{H}(\mathbf{B}) = H_x(\mathbf{B})\vec{e}_x + H_y(\mathbf{B})\vec{e}_y$. For the measurements the rolling direction of the sample was placed into the x-direction. For this purpose, the measurements depicted in Fig. (4) are extrapolated with regression splines over amplitude and angle. Consecutively, the surfaces are created by linear interpolation between the scattered points in polar coordinates. The data points are finally stored in cartesian coordinates, which needs to be interpolated two dimensionally to evaluate the material characteristic in the nonlinear iteration process of the FEM. Moreover, the reluctivity and the differential reluctivity can be

directly computed from the H surfaces. The reluctivity is defined as in Equation (1). For ideal isotropic materials this value is a scalar. In not ideally isotropic materials the reluctivity has to be evaluated in form of a tensor as in Equation (2).

$$\nu = \frac{\mathbf{H}}{\mathbf{B}} \tag{1}$$

$$\boldsymbol{\nu} = \begin{pmatrix} \frac{H_x}{B_x} & \frac{H_x}{B_y} \\ \frac{H_y}{B_x} & \frac{H_y}{B_y} \end{pmatrix} \tag{2}$$

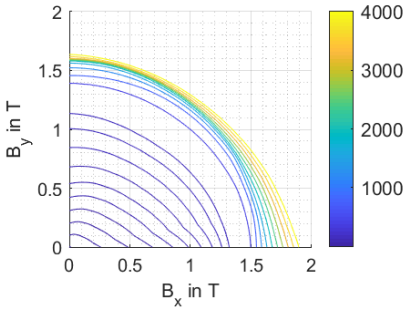

a) $\mathbf{H}_{amp}(B_x, B_y)$

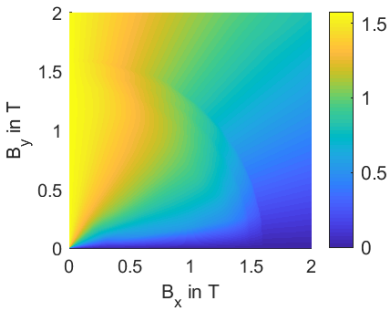

b) $\mathbf{H}_{ang}(B_x, B_y)$

Figure 5: H(B) Surfaces derived from RSST measurements.

For the differential reluctivity, Equation (3) must be evaluated.

$$\boldsymbol{\nu}_d = \begin{pmatrix} \frac{\partial H_x}{\partial B_x} & \frac{\partial H_x}{\partial B_y} \\ \frac{\partial H_y}{\partial B_x} & \frac{\partial H_y}{\partial B_y} \end{pmatrix} \tag{3}$$

The anisotropic behaviour of the measured material can be clearly depicted in Fig. (4a). The angular information is shown in Fig. (4b) and is similar to the measured values, for fluxdensities higher than 1.6 T an effect of the extrapolation is visible. In saturation the angular displacement between H and B is assumed to vanish.

3 Magnetostatic Field Calculation

To solve the magnetostatic field problem the Finite Element method with the magnetic vector potential is applied. The problem consists of a domain Ω with a boundary Γ holding unary and binary boundary conditions ($\Gamma = (\Gamma_u \cup \Gamma_b)$). Furthermore subdomains Ω_c exist, in which a current density $\mathbf{J}$ is imposed. The strong formulation for the magnetic vector potential arises from amperes law stated in Equation (4).

$$\nabla \times \mathbf{H} = \mathbf{J} \tag{4}$$

Introducing the magnetic vector potential $\mathbf{A}$ following in Equation (5) and a consecutive substitution into Equation (4) leads to the well-known magnetostatic vector potential formulation (Equation (6)).

$$\nabla \times \mathbf{A} = \mathbf{B} \tag{5}$$

$$\nabla \times \nu(\nabla \times \mathbf{A}) = \mathbf{J} \tag{6}$$

Considering the strong non-linear behaviour of the ferromagnetic material a non-linear iteration scheme must be employed. A widely implemented and established approach is the Newton method [8,9]. Starting from a first linear solving of Equation (6), it is applied by linearizing Equation (6) in the resulting point by a first order tailor approximation. The linearization is stated in Equation (7).

$$P^k \cdot \Delta\mathbf{A}^k = \mathbf{J} - \left(\nabla \times \mathbf{H}(\mathbf{B})\right) \tag{7}$$

P^k is the Jacobian Matrix, which contains the derivation of the material characteristics and ΔA^k is the correction of $\mathbf{A}$ in iteration step k. For ideal isotropic regions the Taylor approximation can be calculated by Equation (8).

$$\frac{\partial \mathbf{H}}{\partial \mathbf{B}} = \frac{\partial \nu}{\partial \mathbf{B}^2} 2\mathbf{B}^2 + \nu \tag{8}$$

In anisotropic regions the differential reluctivity holds the material information for the Jacobian. For evaluation of H(B) the surfaces for H_x and H_y of the MBMR are used. To receive a unique solution the Coulomb Gauge, stated in Equation (9), must be fulfilled, besides the boundary conditions. For the two-dimensional simulation this gauge condition is implicitly satisfied.

$$\nabla \cdot \mathbf{A} = \frac{\partial A_z(x,y)}{\partial z} = 0 \tag{9}$$

If the rolling direction in the simulation should not be in the x-direction but an arbitrary vector in the x-y plane a coordinate transformation must be considered. The change of the coordinate system can be evaluated inside the non-linear solving procedure or in the pre-processing stage. If it should be calculated in the processing stage the cartesian vector has to be transformed into a new system with rolling and transverse direction as basis using Equation (10). In this system $\mathbf{H}$, $\boldsymbol{\nu}$ and $\boldsymbol{\nu}_d$ have to be evaluated and finally transformed back into the cartesian system by Equations (11) and (12). Replacing $\boldsymbol{\nu}$ by $\boldsymbol{\nu}_d$ in Equation (12) holds the back transformation for the differential reluctivity tensor.

$$\mathbf{B}_{rdtd} = \begin{pmatrix} \cos(\alpha) & \sin(\alpha) \\ -\sin(\alpha) & \cos(\alpha) \end{pmatrix} \cdot \mathbf{B}_{xy} \tag{10}$$

$$\mathbf{H}_{xy} = \begin{pmatrix} \cos(\alpha) & -\sin(\alpha) \\ \sin(\alpha) & \cos(\alpha) \end{pmatrix} \cdot \mathbf{H}_{rdtd} \tag{11}$$

$$\mathbf{v}_{xy} = \begin{pmatrix} \cos(\alpha) & -\sin(\alpha) \\ \sin(\alpha) & \cos(\alpha) \end{pmatrix} \cdot \mathbf{v} \cdot \begin{pmatrix} \cos(\alpha) & \sin(\alpha) \\ -\sin(\alpha) & \cos(\alpha) \end{pmatrix} \tag{12}$$

α is the angular offset of the materials rolling direction towards the x-axis. It can be seen, that the transformations have to be evaluated in every element in each iteration step and therefore produce a big computational effort. By turning the material surfaces for each region in the preprocessing stage this computation effort can be avoided. The presented method and material model are implemented in the software package iMOOSE, developed by the Institute of Electrical Machines RWTH Aachen (IEM).

4 Segmentation and Simulation

In the design process of electrical machines many factors need to be considered. Besides global values like torque and losses the production costs are also important. Therefore, the material waste in the production should be decreased, particularly relating to cutting of the steel laminations. Usually, if stator and rotor consist of the same material, both are punched simultaneously, depicted in Fig. (6a).

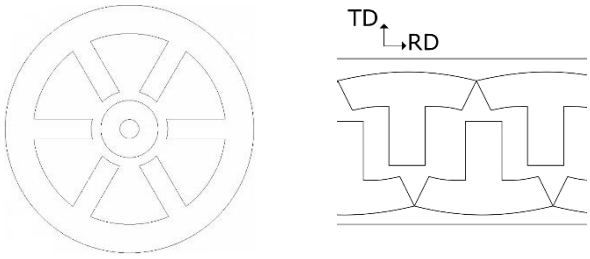

a) Conventional Cutting

b) Cutting of segments e.g. single teeth

Figure 6: Different cutting method for steel laminations used in electrical machines; a) not segmented, b) segmented.

Since the rotor experiences high centrifugal forces, while guiding unidirectional fields, the stator guides rotational fields. These facts and the anisotropic material properties are focus of research and industry [3, 10-12].
The segmentation of the laminations used for the stator can be done as depicted in Fig. 6 b). Next to a stator segmentation the principle can be applied to the rotor if the mechanical properties can be guaranteed. On the one hand, the assembly of segmented machines needs automated processes and is more complicated due to larger amount of pieces compared to the conventional method. On the other hand, the segmented pieces lower the requirements regarding the stamping and the material consumption and thus the material cost are significantly reduced. Additionally, the manufacturing of the single teeth allows the coil to be wound around it resulting in 20 to 30 percent higher slot filling rates [3]. The manufacturing of segmented machines can produce parasitic effects like secondary airgaps between the segments and higher losses due to the increased number of cut edges. Because of the secondary airgaps the segmentation should be applied to machines, that are not sensitive to small deviation regarding the airgap.

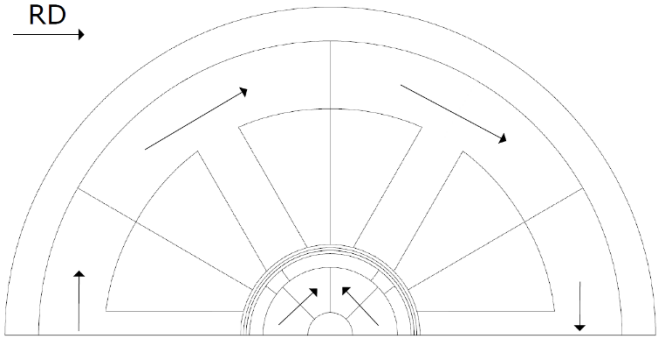

Figure 7: Segmented Synchronous Machine. The arrows indicate the rolling direction of the steel sheets / segments.

In the following the machine depicted in Fig. (7) is simulated. The magnets are mounted onto the rotor laminations and the upper magnet has an outward magnetization, while the ones on the side have an inward magnetization. To use the anisotropy of the material the segmentations of the rotor are assembled in such a way, that the easy magnetization axes is placed in the direction from the side magnets to the upper one. Due to geometrical symmetry and by using binary boundary conditions only one half of the machine has to be modelled. The stator segments have their easy direction as shown in Fig. (6 b). Three different cases are studied in terms of field distribution and torque. The first case is simulated in a conventional way assuming isotropic material behaviour. This approach is used if the machine is fabricated in conventional way as in Fig. (6 a), with a scalar representation of the material. The scalar characteristic was achieved by averaging the measurements in rolling and transverse direction. The material characteristic is shown in Fig. (8).

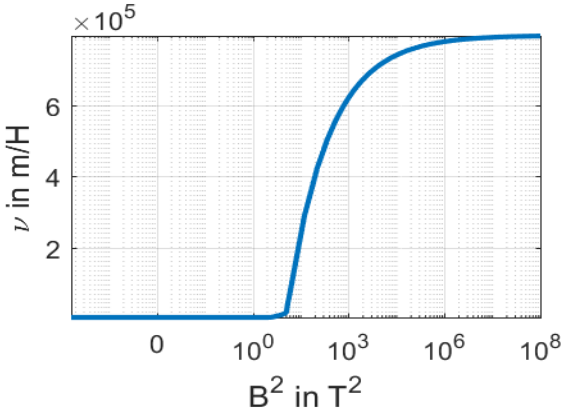

Figure 8: Scalar material characteristic of FeSi-2.4%

The second case considers the magnetic anisotropy, but the entire geometry is oriented to the rolling direction along the x-axis, representing the simultaneous cutting method and no

phase shifting of the laminations in the stacking process. The third simulation takes the segmentation with anisotropy into account, shown in Fig. (7). For all cases the direct current i_d is set to 0 A, while the quadrature current i_q equals 5 A.

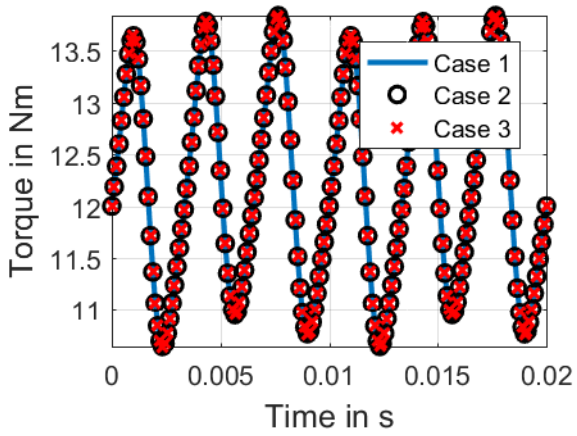

Figure 9: Torque of the presented machine with: Case 1 – Isotropic material, Case 2 - anisotropic material without segmentation, Case 3 – Anisotropic material with segmentation.

In Fig. (9) it is shown, that the deviation in means of torque is negligible small. Case 1 produces the highest torque and Case 2 and 3 are less than 0.1 % smaller when compared to the reference. This is due to the fact, that the field in the ferromagnetic parts is different for all cases and the air gap is the only location in which the electromagnetic energy conversion takes place.

To further analyse the influence of anisotropic material on the field distribution the solution for the first-time step is depicted in Fig. (10). It can be perceived, that the flux density in the yoke and the region at the teeth roots is considerably different, but the flux density in the airgap is approximately the same. This confirms the consideration stated above regarding the torque. Further due to different material characteristics in each segment due to the phase shift drawn in Fig. (7), the lines of equipotential show a refractive behaviour due to the interface conditions of the field quantities.

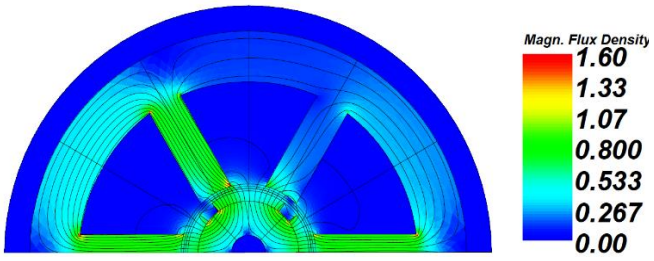

a) Isotropic Material – Case 1

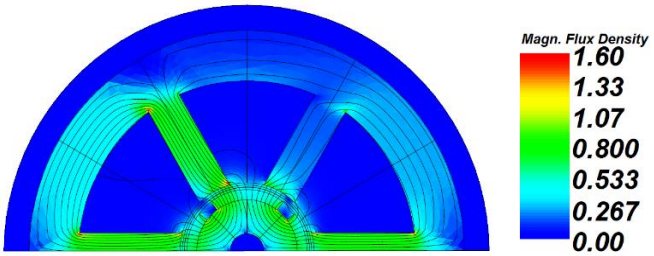

b) Anisotropic Material – Case 2

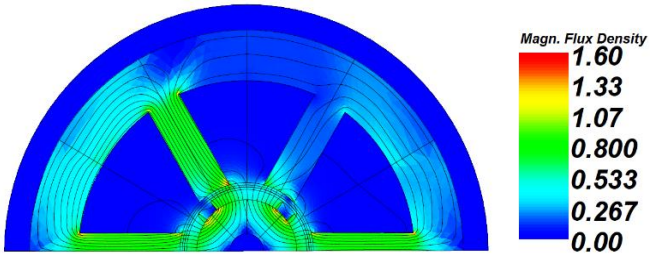

c) Anisotropic Material Case 3

Figure 10: Field distribution: Case 1 – Isotropic material, Case 2 - anisotropic material without segmentation, Case 3 – Anisotropic material with segmentation

The equipotential lines in Fig. (10 b) and (10 c) clearly show the influence of the anisotropy. For Case 2 the easy direction lies in the x-axis and the transversal direction in the y- axis. The equipotential lines show the path of the flux density, indicating the easiest path for the flux. For e.g. the root of the tooth in 120 degree reveals this in form of a different shape of the curvature of the equipotential lines. The third case shows the biggest deviation due to the many different directions and material interfaces.

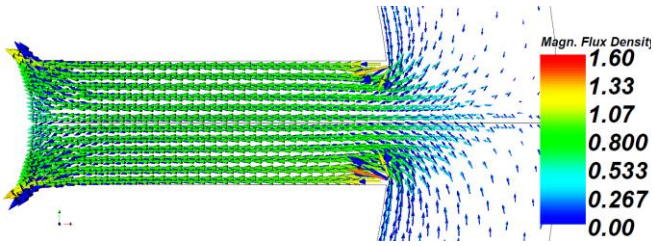

a) Phase lag between H (blue) and B

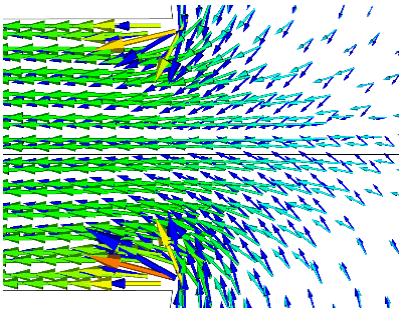

b) Phase lag in the tooth root of H (blue) and B

Figure 11: Vectorial behaviour of H and B in the tooth at one time step.

Besides the consideration of the directional dependent material behaviour the MBMR allows for simulation of angular shifted vectorial quantities of **H** and **B**, which can be directly found in the measurements. The phase lag between **H** and **B** is depicted in Fig. (11). **H** and **B** are collinear in the middle of the tooth and it can be clearly recognized, that the angular displacement shows a maximum in the tooth root and the tooth tip.
In Fig. (12) the Loci for **B** and **H** are shown for an element in the tooth root. While the isotropic material results in an elliptical locus, the anisotropic material does not. The peaks in the H locus in Fig. (12b) come from the measured data and can be smoothed by measuring in smaller angular steps.

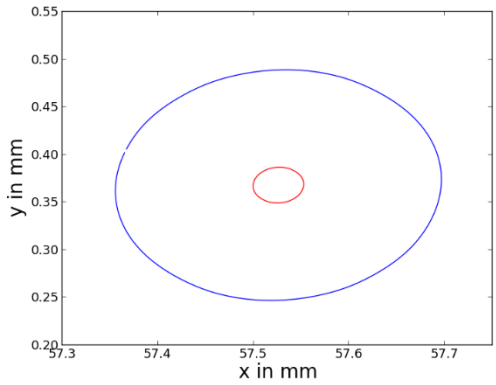

a) Isotropic

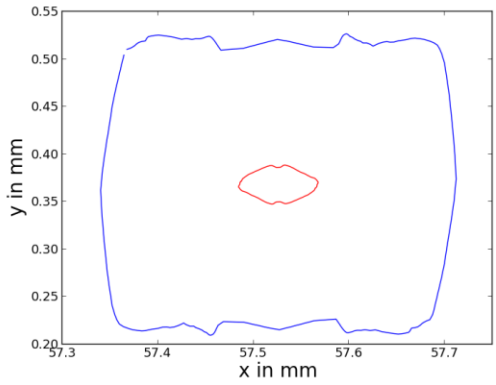

b) Anisotropic (MBMR)

Figure12: B- (red) and H-Loci (blue) for isotropic and anisotropic material; 1 mm is equal to 200 A/m and 9 T.

5 Conclusions

The segmentation of electrical machines offers striking improvements regarding modulation, automated production and material savings. Due to the not ideally isotropic behaviour of electrical steel sheets anisotropy is always present. In this paper a measurement based tensorial material representation was introduced and applied to a small-scale synchronous machine. Even though the torque is not noticeably influenced the field distribution deviated clearly from the isotropic case. Therefore, focus of future work will be the loss estimation with consideration of anisotropy and angular displacement between H and B, as well as incorporation of hysteresis.

Acknowledgements

This work was supported by the Deutsche Forschungsgemeinschaft (DFG) within the research project number 373150943 “Vector hysteresis modeling of ferromagnetic materials” and 255713208 “FOR 1897 – Low-Loss Electrical Steel for Energy-Efficient Electrical Drives”.

References

[1] N. Leuning, S. Steentjes, K. Hameyer. “On the Homogeneity and Isotropy of Non-Grain-Oriented Electrical Steel Sheets for the Modeling of Basic Magnetic Properties from Microstructure and Texture”, IEEE Transactions on Magnetics, vol. 53, (2017).

[2] B.D. Cullity, C.D. Graham. *Introduction to magnetic materials*, Hoboken, N.J., IEEE/Wiley, (2009).

[3] A. N. El-Refaie. “Fractional-Slot Concentrated-Windings Synchronous Permanent Magnet Machines: Opportunities and Challenge”, *IEEE Transactions on Industrial Electronics*, **vol. 57,** pp. 107-121, (2009).

[4] A. Thul, S. Steentjes, B. Schauerte, P. Klimczyk, P. Denke, K. Hameyer. “Rotating magnetizations in electrical machines: Measurements and modeling”, *AIP Advances*, **vol. 8**, no. 5, p. 56815, (2018).

[5] F. Fiorillo, I. D. Mayergoyz. *Characterization and Measurement of Magnetic Materials*, Burlington: Elsevier (2004).

[6] F. J. G. Landgraf, T. Yonamine, M. Emura, M. A. Cunha. “Modelling the angular dependence of magnetic properties of a fully processed non oriented electrical steel”, *JMMM*, **vol. 254-255**, pp. 328-330, (2003).

[7] J. Barros, J. Schneider, K. Verbeken, Y. Houbaert. „On the correlation between microstructure and magnetic losses in electrical steel”, *Journal of Magnetism and Magnetic Materials*, **vol. 320**, pp. 2490-2493, (2008).

[8] J. Gyselinck, P. Dular, N. Sadowski, J. Leite, J.P.A. Bastos. “Incorporation of a Jiles-Atherton vector hysteresis model in 2D FE magnetic field computations”, *COMPEL*, **vol. 23**, pp. 685-693, (2004).

[9] C. Krüttgen, S. Steentjes, G. Glehn, K. Hameyer. “Parametric homogenized model for inclusion of eddy currents and hysteresis in 2-D finite element simulation of electrical machines”, *IEEE Transactions on Magnetics*, **vol. 53**, pp. 1-4, (2017).

[10] D. Platt, “Reluctance motor with strong rotor anisotropy”, *IEEE Transactions on Industry Applications*, **vol.28**, pp. 652-658, (1992).

[11] S. Taghavi, P. Pillay, “A Novel Grain-Oriented Lamination Rotor Core Assembly for a Synchronous Reluctance Traction Motor With a Reduced Torque Ripple Algorithm”, *IEEE Transactions on Industry Applications*, **vol. 52**, pp. 3729-3738, (2016).

[12] S. Lopez, B. Cassoret, J. F. Brudny, L. Lefebvre and J. N. Vincent. "Grain Oriented Steel Assembly Characterization for the Development of High Efficiency AC Rotating Electrical Machines", IEEE Transactions on Magnetics, **vol. 45**, pp. 4161-4164, (2009).